AIAA 2002-0267

Micro Electro Kinetic Actuator (MEKA) Arrays for Active Sublayer Control of Turbulent Boundary Layers

Francisco J. Diez and Werner J.A. Dahm

Laboratory for Turbulence & Combustion (LTC)
Department of Aerospace Engineering
The University of Michigan
Ann Arbor, MI 48109-2140

Micro Electro Kinetic Actuator (MEKA) Arrays for Active Sublayer Control of Turbulent Boundary Layers

Francisco J. Diez[1] and Werner J. A. Dahm[2]

Laboratory for Turbulence & Combustion (LTC)
Department of Aerospace Engineering
The University of Michigan
Ann Arbor, MI 48109-2140

Recent progress is summarized in the development of microactuator arrays that function on the electrokinetic principle to permit active control of streamwise sublayer vortical structures in turbulent boundary layers. Electrokinetic microactuator arrays induce volume displacement in the sublayer by electrokinetic pumping under an impulsively applied electric field. Individual microchannels are formed in a substrate and filed with a 1 μm-scale doped porous polymer matrix material that provides the required ζ-potential when wetted by the corresponding electrolyte. The resulting microactuator arrays have many characteristics that make them potentially suited for practical sublayer control on full-scale aeronautical and hydronautical vehicles. Essentially loss-less frequency response has been demonstrated to 10 kHz. Several such micro electrokinetic actuator (MEKA) arrays have been fabricated from a three-layer design leading to the MEKA-5 full-scale hydronautical array, composed of 25,600 individual electrokinetic microactuators with 350 μm center-to-center spacings, arranged in a 40×40 pattern of unit cells, each composed of a 4×4 matrix of actuators; this array was successfully fabricated in a 7×7 cm^2 tile in 250 μm thick mylar substrate material. MEMS design and fabrication processes were used to produce a top layer for the MEKA-5 hydronautical-scale array; the functionality incorporated in this top layer fabrication demonstrates the complete elements needed for microscale electrokinetic actuator arrays for sublayer control.

1. Introduction

Active control for drag reduction on aeronautical and hydronautical vehicles is among the highest-impact applications of microsystems technology for military and commercial purposes, and represents one of the longest-standing objectives in the field of fluid dynamics. A reduction in the drag on an air vehicle of just a few percent translates into enormous system-wide reductions in fuel weight and operations costs, and corresponding increases in vehicle range and payload delivery. Similarly, flow control devices capable of on-demand vortex generation over delta wings, strakes, and other control surfaces in fighter aircraft would permit dramatic increases in maneuverability, and large reductions in radar cross-section through elimination of traditional control surfaces. Such benefits of microsystems-based flow control extend to naval surface and undersea vehicles as well, including ships, submarines, and torpedoes, as well as to unmanned vehicles used in a variety of applications such as UAV's, UCAV's, and MAV's. Similar technologies could be also applied to supersonic vehicles for aerodynamic noise reduction, and would find use in a wide range of flow control situations involved in propulsion systems, spanning from control of mixing in advanced gas turbine combustors, to active control of surge and stall in compressors.

The extensive development of micro-electro-mechanical-systems (MEMS) technologies over the past decade has opened a new avenue for such active control approaches. One approach for controlling the vehicle boundary layer is to exploit the streak-like vortical structures that exist naturally in the viscous sublayer of turbulent boundary layers to achieve drag reduction. MEMS fabrication processes allow comparatively inexpensive production of large, dense arrays of microscale wall shear stress sensors and pressure sensors, typically having length scales of the order of a few hundred μm. Such sensor arrays are, in principle, capable of detecting the wall signature of the instantaneous coherent structure pattern in the near-wall region of turbulent boundary layers. Information of this type could, in principle, be used with large dense arrays of MEMS-fabricated

1. Graduate Student; AIAA Student Member.
2. Professor; AIAA Senior Member; Corresponding author.

wall actuators and an appropriate control system to manipulate the near-wall coherent structures and their dynamics so as to interfere with the bursting process. Various attempts to develop sensors, actuators, and control systems to accomplish this goal are discussed by Bushnell & McGinley (1989), Fiedler & Fernholz (1990), Wilkinson (1990), Gad-el-Hak (1989, 1994, 1996, 2001), Choi *et al* (1993, 1994), Jacobson & Reynolds (1993, 1998), Moin & Bewley (1994), McMichael (1996), Lumley (1996), Ho & Tai (1996, 1998), Pollard (1997), Lumley & Blossey (1998), and Löfdahl & Gad-el-Hak (1999).

The studies noted above have shown that active sublayer control of turbulent boundary layers is feasible under laboratory conditions, and have demonstrated several types of actuators suitable for active sublayer control under laboratory conditions. However unlike such laboratory-scale demonstration experiments, the turbulent boundary layers on real aeronautical and hydronautical vehicles are typically at much higher Reynolds numbers, and thus involve much smaller length scales and much shorter time scales than are generally achievable in laboratory-scale boundary layers. Furthermore, actuator arrays on real vehicles will be subjected to a variety of non-ideal environmental and operating conditions that are not encountered under laboratory conditions. Practical microactuators for use on vehicles will thus need to be sufficiently robust and infragile to permit operation under such conditions. Finally, the power requirements for large, dense arrays of such microactuators to achieve the desired level of drag reduction must be sufficiently small to provide a significant net reduction in the power requirements of the vehicle. All of these factors complicate the practical application of existing microactuator technologies to permit active sublayer control for drag reduction on full-scale vehicles under realistic operating conditions. In this paper, we describe the first use of the electrokinetic principle (e.g., Potter 1961) as the basis for an entirely new class of microactuators for integration in large arrays to meet the requirements for sublayer control in turbulent boundary layers on vehicles (Dahm et al 1997).

2. Microactuator Performance Requirements

The bursting process associated with streamwise vortices at the outer edge of the viscous sublayer sets the rate of momentum transport from the wall to the fluid, and hence the drag that acts on the vehicle. Drag reduction can be accomplished by acting on the streamwise vortices to interrupt or otherwise interfere with this sublayer bursting process. For the present microactuator arrays, the individual actuators serve as point volume sources that impulsively displace a fixed volume of fluid in the near-wall region of the flow. Each actuator thus produces locally positive or negative volume displacements over a brief time interval to displace the streamwise sublayer vortices along the spanwise direction. The performance requirements of individual microactuators needed to achieve such lateral displacement of the sublayer vortices is based on the structure and dynamics of the near-wall region of turbulent boundary layers (Diez-Garias et al 2000). It then uses this information to derive the actuator spacing, frequency, and flow rate requirements necessary to achieve adequate displacement of individual sublayer vortical structures.

Irrespective of the control approach used and the microactuator type it implies, it is necessary to have an array of actuators that allow the streamwise sublayer vortices to be acted upon appropriately. Key performance requirements involve the microactuator spacing, frequency, and flowrate needed to achieve adequate displacement of individual sublayer vortical structures. For closed-loop control approach based on individual point microactuators, from the forgoing summary of the sublayer vortex structure and dynamics it is apparent that such actuators must be separated by typically 100 wall units, and displace a volume of fluid with an equivalent hemispherical radius of the order of 10 wall units l_τ

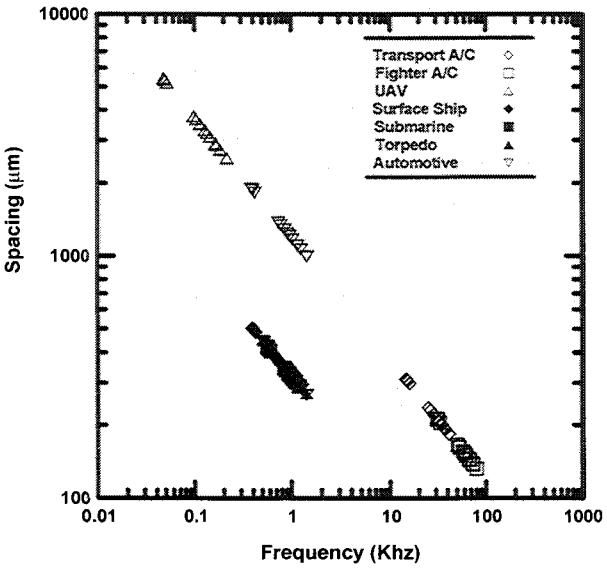

Fig. 1. Microactuator spacing and frequency requirements for active sublayer control by manipulation of streamwise vortical structures, showing results for different aeronautical and hydronautical vehicles. Note that hydronautical applications all require microactuator arrays with approximately 300 μm actuator spacings and 1 kHz frequency response.

with a step response that corresponds to a scaled frequency of $f^+ = 10^{-2}$.

With this information, it is possible to determine the size and performance requirements to which these conditions correspond for various types of vehicles. These performance requirements will depend on the fluid type (principally air or water, which differ in their density and viscosity), on the vehicle speed, and on the vehicle length. More precisely, the universal structure and scaling of equilibrium turbulent boundary layers shows that the local sublayer properties, and hence the local microactuator performance requirements, depend on the local boundary layer thickness δ, the local fluid speed U at the "edge" of the boundary layer, the local pressure gradient dp/dx, and the fluid properties ρ and μ. Of these, the direct effect of the pressure gradient is relatively weak; it is the indirect effect of the pressure gradient on the boundary layer thickness δ that dominates. This permits an analysis for each vehicle type without requiring a detailed boundary layer calculation for a specific vehicle geometry. In effect, the performance requirements can be obtained at any streamwise position on the vehicle for a variety of pressure gradient parameters Π ranging from strongly favorable to moderately adverse.

Accordingly, Fig. 1 shows the results obtained for the required point microactuators spacing and frequency response at four downstream locations (x/L = 0.25, 0.5, 0.75, and 1.0) and for four different pressure gradients. It is apparent, both from the results shown and from fundamental considerations, that vehicle speed is the principal factor that drives both the actuator spacing and frequency requirements. These requirements are relatively benign for the UAV application, where actuator spacings of several millimeters and step response of 100 Hz are sufficient to act on virtually every sublayer streak. At the other extreme, the supersonic fighter and transport aircraft require actuator spacings of 100-200 μm and step response of 10-90 KHz. The various hydronautical applications, which differ from the aeronautical applications due to the $O(10^{-3})$ lower kinematic viscosity, require microactuator spacings around 300 μm but frequencies of only about 1KHz.

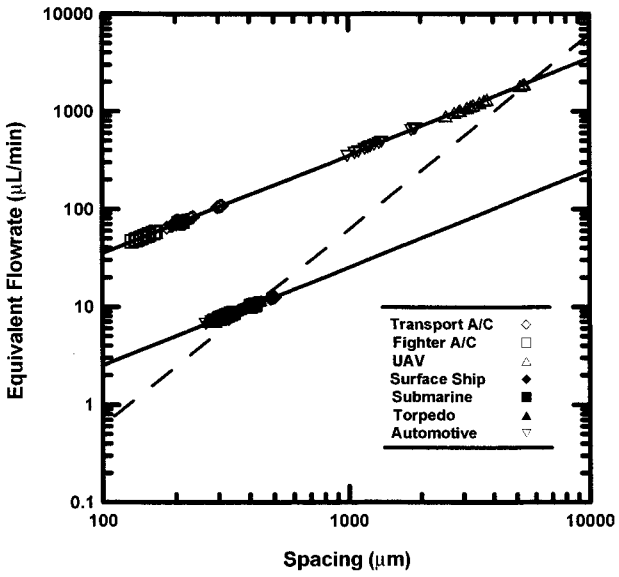

Fig. 2. Microactuator flow rate and spacing requirements for active sublayer control by manipulation of streamwise vortical structures. The dashed line shows coupling between microactuator spacing and flow rate corresponding to simple geometric scaling of any given microactuator design. Increased actuator spacings provide increased area for electrokinetic pumping channels, which in turn provide for larger volume flow rates.

For electrokinetic microactuators that are intended for use in dense arrays, the maximum flow rate achievable by each actuator is limited by the area per actuator available for the electrokinetic pumping channels. As a consequence, the flow rates are closely connected with the microactuator spacing. This is shown in Fig. 2, where the maximum flow rate achievable is shown as a function of the spacing between individual microactuators within the array. The dashed line shows the result for simple geometric scaling of a given actuator design, for which the flowrate Q increases as actuator spacing l as $Q \sim l^2$. The implication of this is that a microactuator array designed for use in full-scale hydronautical applications can simply be geometrically scaled up in size by a factor of 15 to provide the required microactuator array for a UAV-scale aeronautical application. The other aeronautical applications, however, would require microactuator arrays that can achieve electrokinetic pumping efficiencies, namely higher values of the equivalent DC flowrate Q per unit microactuator area l^2. For this reason the MEKA-5 microactuator array developed in thus study (see §5) has been designed for full-scale hydronautical applications, with 25,600 individual electrokinetic microactuators arranged on 325 μm center-to-center spacings in a 7 × 7 cm^2 array. The same array can be directly scaled up – with no increase in per-actuator performance required – for the UAV-scale application.

3. System Architecture for Microactuator Arrays

The typically 300 μm spacing between microactuators required for hydronautical vehicles of 100 m scale, such as a submarine hull, implies that of the order of 30 billion individual microactuators would be required to cover the entire vehicle surface. The massive difficulty of integrating such a large number of actuators, with a

comparably large number of sensors and an appropriate control processing capability, can be greatly simplified by taking advantage of the inherently local nature of the sublayer structure and dynamics. In particular, the length of the sublayer vortices typically extends over only about 1000 wall units l_τ, and the bursting process occurs between adjacent counter-rotating pairs of these vortices that are typically separated along the spanwise direction by only about 100 wall units l_τ and are typically located about 10 wall units l_τ above the wall as described by Diez-Garias et al (2000). Moreover, the bursting process itself is principally dependent on the separation between the pair of counter-rotating sublayer vortices, and is largely independent of the locations and dynamics of other distantly-located sublayer vortices. This inherent locality suggests that sublayer control of the turbulent boundary layer over the entire vehicle can be broken down into elementary "unit cells", the size of which is set by these length scales associated with the bursting process. Moreover, this also suggests that dynamical interactions between such unit cells should be comparatively weak in relation to the interactions between sublayer vortices within a given unit cell. Any such interactions would extend at most to the next adjacent unit cells, and to a good approximation such cell-to-cell interactions could be neglected altogether. The unit cells then become fully independent, each with their own sensors, control processing, and actuators. Since the number of sensors and actuators within such unit cells is then relatively small, the problem of integrating them into a complete control system becomes correspondingly simpler.

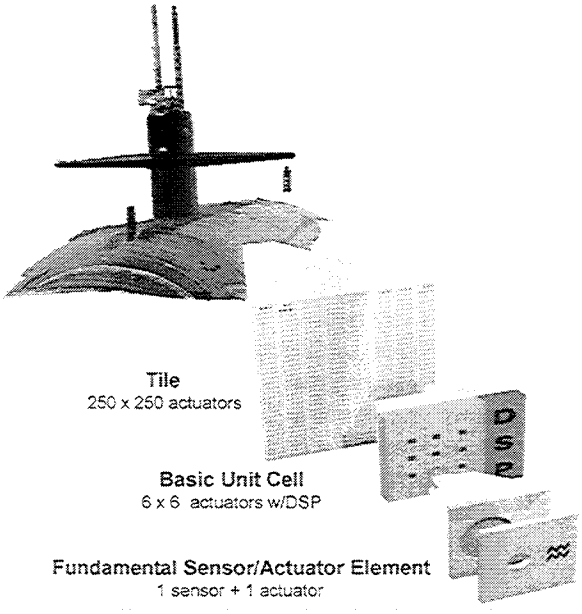

Fig. 3. Schematic indicating fundamental architecture for microactuator arrays based on a unit-cell structure developed in this study. Each unit cell is composed of small arrays of sensors and actuators, with local unit-cell control processing capability resident in each cell. Tiles containing large numbers of such units cells can be produced using microfabrication techniques.

The fundamental size of the unit cells in this system architecture is 500 l_τ in both the streamwise and spanwise directions (see Diez-Garias 2002). Moreover, the 500 $l_\tau \times$ 500 l_τ unit cells in this architecture are taken to be completely independent of each other, though cell-to-cell interactions between adjacent unit cells could be readily incorporated by having each of the cell-based control processors share information with adjacent cells. Figure 3 schematically shows how this concept can be used to group the sensors, actuators, and processing over an entire vehicle into such unit cells, each composed of an $n \times n$ arrangement of elementary sensor and actuator pairs together with local unit-cell processing capability. Given the unit-cell dimensions noted above and the actuator spacings shown in Fig. 2, it is apparent that n will typically be in the range of $4 \le n \le 6$.

Furthermore, the relatively small number n^2 of sensor-actuator pairs in each such unit cell allows the resident processing capability that "connects" these sensors and actuators to be greatly simplified. While most previous work has examined comparatively elaborate control processing approaches based on fundamental control theory, many of which require comparatively sophisticated local processing capability to implement, the unit-cell approach permits investigation of potentially far simpler methods. In particular, the number of sensors and actuators is sufficiently small that true "processing" at the unit-cell level may be discarded entirely, and replaced by a simple "look-up table" approach. In this case, the actuator states are directly implied by the sensor states via a look-up table stored in a simple programmable logic array (PLA) in each unit cell. In this manner, on each clock cycle the new sensor states are used to determine the new actuator states, thus eliminating the need for any true processing capability.

Moreover, given the typical dimensions of these unit cells and the dimension of the silicon wafers on which microfabrication technologies, such as photolithography and other MEMS processes, can be used to parallel-fabricate large numbers of such unit cells, it is natural to group these unit cells into "tiles", as also shown in Fig. 3. Each tile contains the number of unit cells that can be fit into a square array on a single wafer. For typical unit-cell sizes and wafer sizes, this dictates roughly 250 $\times$ 250 unit cells in each tile. Each tile has a single pair of electrical leadouts, with an internal bus structure that distributes power to each of the unit cells. These tiles

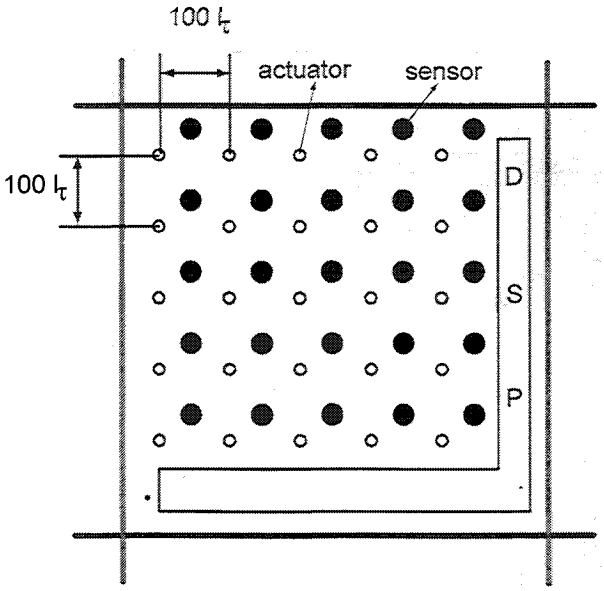

Fig. 4. Basic unit-cell architecture, showing collocated $n \times n$ arrays of typically $4 \le n \le 6$ microscale sensors and actuators spaced 100 viscous wall units l_τ apart, with space for unit-cell processing and with common voltage bus lines separating adjacent unit cells. The relatively small number of sensors and actuators in each unit cell permits simple look-up table approaches for the unit-cell processing.

form the basic elements used to cover desired parts of the vehicle surface on which sublayer control is to be accomplished.

As indicated in Fig. 4, each unit cell in this system architecture is composed of a collocated array of wall shear stress sensors, electrokinetic microactuators, and local digital signal processing (DSP) capability. This section briefly describes the key aspects of the major components that make up each of the fully-independent unit cells on each tile, consisting of an $n \times n$ array (with typically $4 \le n \le 6$) of sensors and actuators connected via the unit-cell control logic.

Each unit cell contains an $n \times n$ array of electrokinetic actuators that provide the volume displacement within the near-wall region of the turbulent boundary layer to laterally displace the streamwise sublayer vortices. Although the fundamental unit-cell architecture can accommodate essentially any type actuator, the electrokinetic microactuators that are the principle focus of this study offer several benefits that make them potentially well suited for active sublayer control. The electrokinetic principle on which these microactuators function (see §4) requires no moving parts, with the volumetric pumping being induced by an impulsively applied electric field. As a result, these electrokinetic microactuators can be significantly more robust than many other actuators based on moving parts. Moreover, the scalings that govern the electrokinetic effect provide significant performance advantageous for actuators fabricated at the microscale. In particular, such electrokinetic microactuators can achieve an extremely high impulse response, and equivalent steady flow rates sufficient to meet the requirements noted in §2 for active sublayer control under full-scale vehicle operating conditions. Such microactuators can also be readily sized to fit with the unit-cell architecture, and do not involve any parts that protrude into the flow.

Furthermore, such electrokinetic microactuators can be fabricated with a comparatively simple three-layer design, as indicated in Fig. 5. This design involves a top layer containing the individual actuator nozzles and electrodes together with leadouts to the unit-cell DSP, a middle layer containing the electrokinetic driver channels filled with a porous polymer matrix in which pumping of the electrolyte occurs, and a bottom layer that serves as a common electrolyte reservoir for the unit cell (or, alternatively, for the entire tile).

4. Electrokinetic Theory

The electrokinetic microactuators that are the subject of this work function on the basis of the electrokinetic effect (*e.g.*, Potter 1961; Burgreen & Nakache 1964), first noted by Reuss (1809). While this effect inherently operates at the microscale, it is widely used in a variety of practical devices and processes to produce macroscale effects. Examples include transport processes in

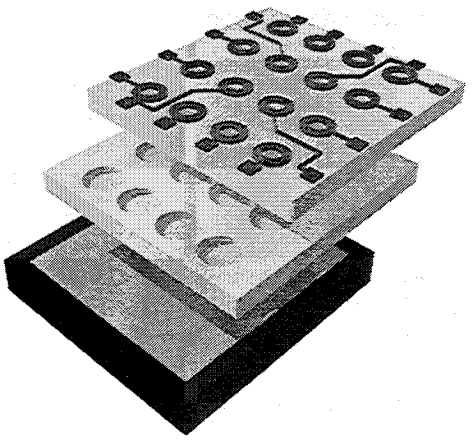

Fig. 5. Fundamental three-layer design of electrokinetic microactuator arrays at the unit-cell level, showing a top layer containing individual actuator nozzles, electrodes and leadouts, a center layer containing the electrokinetic driver channels in which electrolyte pumping occurs in response to an applied electric field, and an electrolyte reservoir and common electrode in the bottom layer.

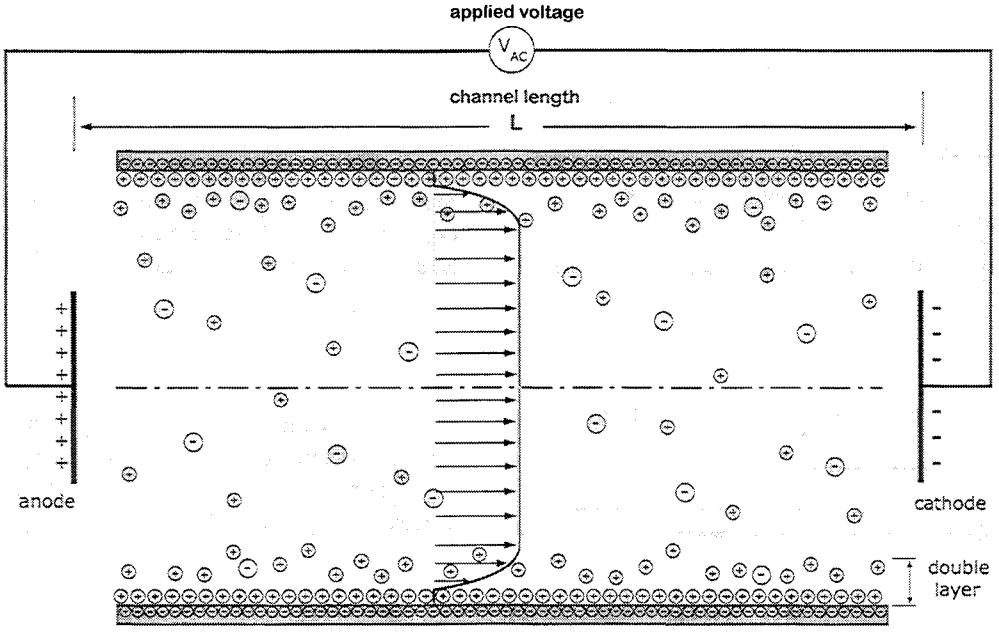

Fig. 6. Schematic showing the electrokinetic flow induced by an applied electric field along a pore or capillary channel. The electric field induces drift in the mobile ions within the diffuse outer layer, which then collisionally transfer momentum to the electrolyte. Subsequent collisional transport (diffusion) transfers this motion throughout the channel.

emulsions and suspensions, as well as soil remediation processes, to name just a few. The present study is the first attempt to exploit its potential advantages as the basis for a new class of microscale actuators suitable for active sublayer control in turbulent boundary layers at full-scale vehicle operating conditions.

The electrokinetic effect occurs at the interface between two phases, typically a solid and a liquid, that are in direct contact with one another. In the case of the present electrokinetic microactuators, this interface is between a solid polymer and an electrolytic fluid. An ionic "double-layer" shown in Fig. 6 forms naturally at such an interface (Diez-Garias 2002). When an electric field is applied to a liquid electrolyte in contact with a charge solid surface, it produces a displacement of the liquid with respect to the stationary surface. In practice, this stationary surface might typically be a thin capillary tube or a fine porous matrix, with the electrolyte filling the open volume.

The Navier-Stokes equation can be used to obtain the detailed outer-layer structure and the resulting electrokinetic pumping that it induces under the influence of an applied electric field (e.g., Burgreen & Nakache 1964, Rice & Whitehead 1965).

For a channel of radius R consisting of $(R/w)^2$ individual pores each of radius w (see Diez-Garias et al. 2000), the flow rate becomes

$$Q = \pi R^2 \Omega E_z, \tag{1}$$

where E_z is the applied electric field and Ω is the ionic mobility and is defined as

$$\Omega = \frac{\varepsilon \zeta}{\mu}. \tag{2}$$

Here ε is the permittivity of the electrolyte, ζ is the potential at the wall of a pore and μ is the electrolyte viscosity.

with the resulting flow speed $U=Q/\pi R^2$, and the force F achieved in a plugged actuator becomes

$$F = 8\pi\mu\Omega\left(\frac{R}{w}\right)^2 E_z L. \tag{3}$$

Benchtop testing conducted with electrokinetic microactuators formed from channels packed with a porous polymer with mean pore size of 1 μm and operated under DC conditions verified the volume displace rate described by (1). Thus, it was observed that Q increases linearly with applied voltage and the ionic mobility Ω (see Diez-Garias 2002 for more details).

Note (1) that the flow rate achieved is independent of the pore radius w, but the force in (3) increases as the pores are made smaller. This suggests and has been verified (Diez-Garias et al. 2000) that by fabricating electrokinetic channels with sufficiently small pores, it is

possible to achieve flow rates adequate to meet the requirements in §2 while at the same time achieving sufficiently high pressures in any plugged actuators to allow these to unplug themselves. Moreover, such electrokinetic actuators fabricated at the microscale have extremely high frequency response owing to the small time scales required for collisional (diffusion) transport of the induced flow across the channel.

5. Elecrokinetic Microactuator Arrays

5.1 *MEKA-5 Hydronautical Array*

Several micro electrokinetic actuator (MEKA) arrays have been fabricated from the three-layer design shown in Fig. 5. This has led to the MEKA-5 actuator array, shown in Fig. 7, which demonstrated fabrication of a full hydronautical-scale array of electrokinetic microactuators and their integration with a top-layer containing the basic unit-cell structure and all electrical leadouts required for actuation. The array was fabricated in a 7×7 cm^2 tile, containing 25,600 individual electrokinetic microactuators with 250 μm channel diameters arranged on 350 μm center-to-center spacings, as indicated in Figs. 2.4 and 2.6 for full-scale hydronautical vehicle applications. These individual electrokinetic microactuators were grouped into 1600 individual unit cells

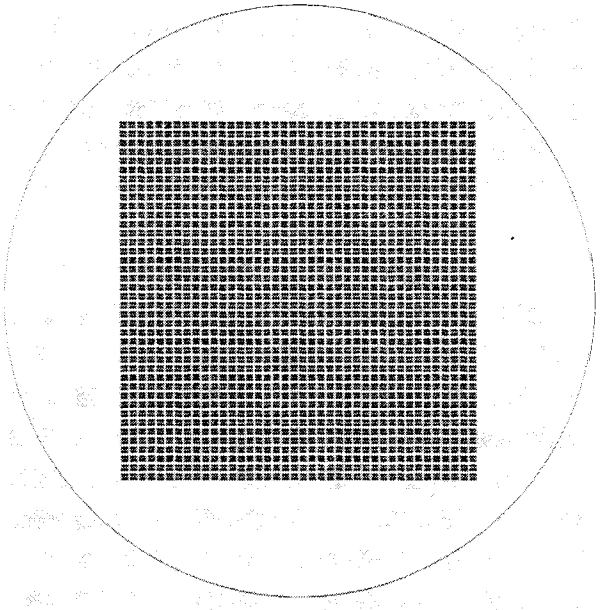

Fig. 7. Layout of electrokinetic microactuator channels in center layer of MEKA-5 full-scale hydronautical array, showing 25,600 individual microactuator channels grouped into a 40×40 pattern of unit cells, each containing a 4×4 unit-cell structure on 325 μm center-to-center spacing. Array is shown at actual size.

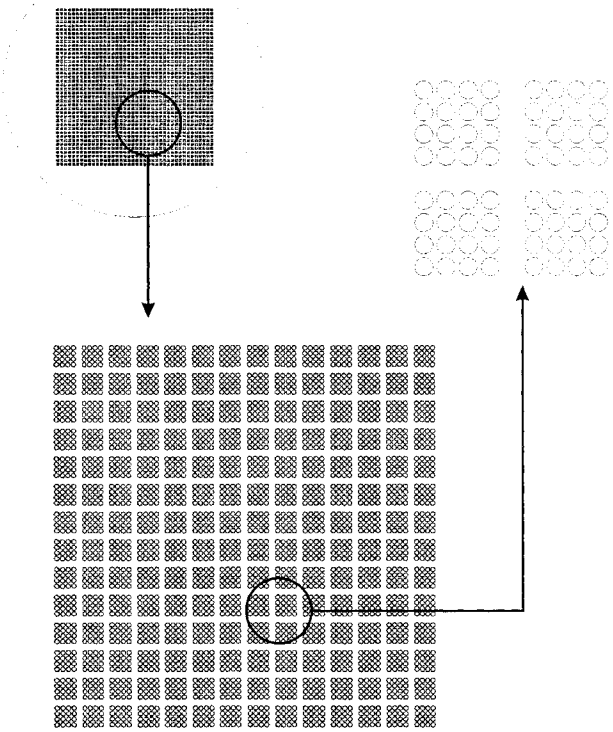

Fig. 8. Unit-cell pattern on the MEKA-5 hydronautical-scale array, showing how full tile is arranged into individual 4×4 unit-cell structures. Every fifth row and column of actuators was skipped to provide space for unit-cell control processing.

arranged in a 40×40 unit-cell pattern on each tile, with each unit-cell composed of a 4×4 array of microactuators. As indicated in Fig. 8, every fifth row and column of microactuators in the tile was skipped to provide room for the resident unit-cell processing electronics. The top layer, shown in Fig. 9*a*, was fabricated using conventional MEMS processing steps. The center layer in Fig. 9*b* was fabricated with the same porous polymer matrix material in thin flexible mylar substrate material suitable for conformal application on a vehicle surface. The following sections describe these center-layer and top-layer fabrication processes used to develop this full-scale MEKA-5 hydronautical array.

5.2 *MEKA-5 Center Layer Fabrication*

Figures 10*a* and 10*b* show the center layer of the three-layer MEKA-5 hydronautical array tile. Each of the 25,600 individual electrokinetic microactuators has a 250 μm microchannel diameter and 350 μm center-to-center spacing between microactuators within a unit cell. The channels were fabricated in flexible mylar substrate material, having 250 μm thickness to permit a high electric field E across the individual actuator chan-

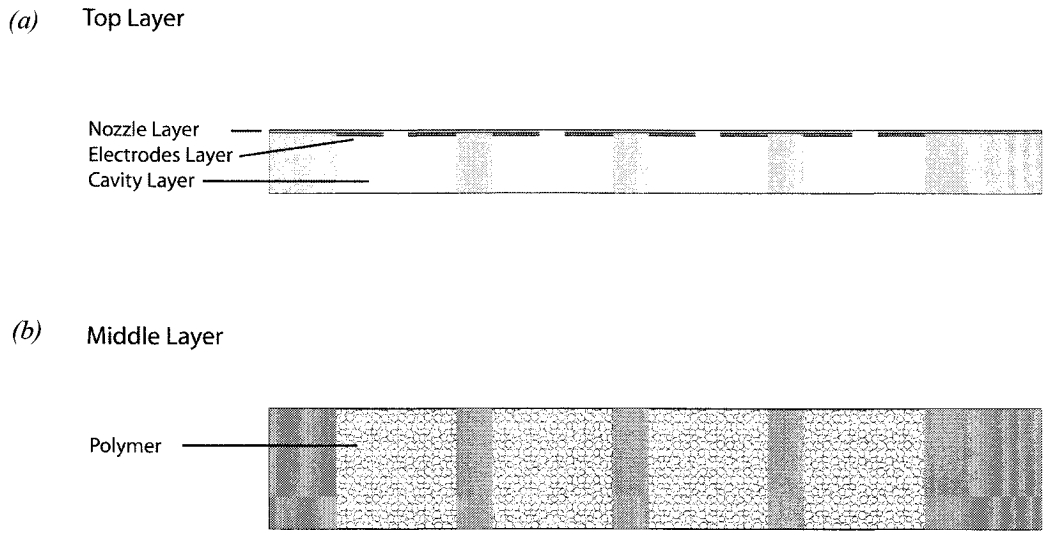

Fig. 9. Basic elements fabricated in 25,600-element MEKA-5 hydronautical-scale array, showing *(a)* top layer with cavities, electrodes and leadouts, and nozzles, and *(b)* center layer with actuator channel and porous polymer matrix. Individual sublayers are shown in Figs. 5.19-5.23. MEMS fabrication process steps are shown in Fig. 5.24.

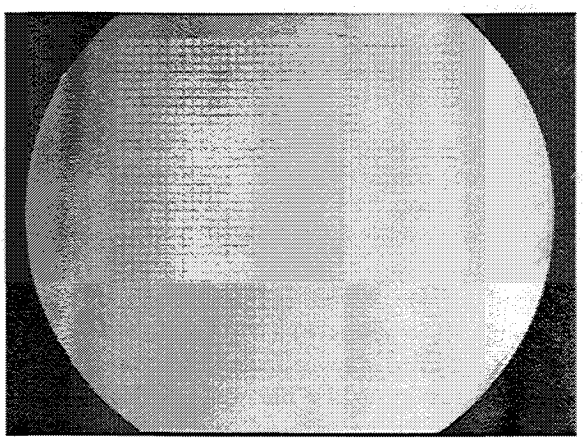

(a)

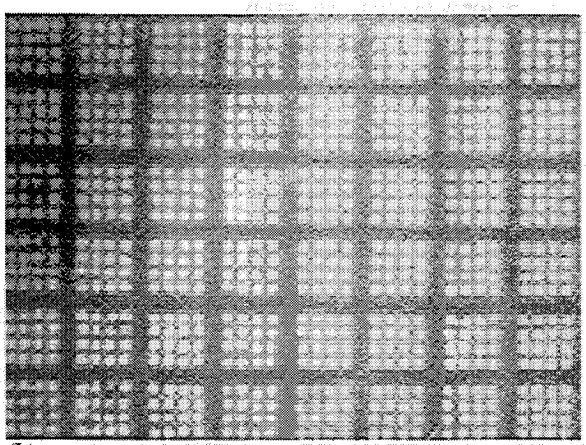

(b)

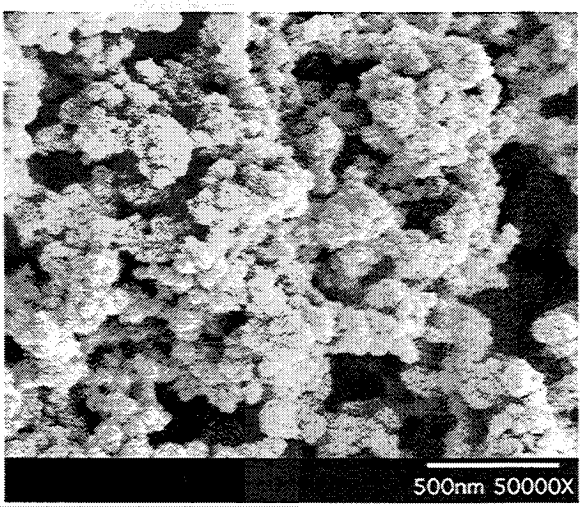

(c)

Fig. 10. (a) Center layer of 25,600-element MEKA-5 hydronautical-scale array fabricated in thin flexible mylar (b) Close-up view of 250 μm diameter actuator channels filled with porous polymer matrix structure in MEKA-5 hydronautical-scale array, showing individual 4 × 4 unit-cells. (c) SEM micron-scale photograph of the porous polymer matrix structure resulting from two-component polymer fabrication process of the type used in the MEKA-5 array.

nels at a low voltage difference. A potential difference of just 20 V across this 250 μm thick center layer produces the necessary field strength to achieve the 10 μl/min equivalent DC flow rate in Fig. 2 needed for active sublayer control on hydronautical vehicles. The electrokinetic porous polymer matrix structure was filled in the liquid state in the microchannels by a two component polymerization process. The curing process produced a porous matrix with pore sizes in the range of 1 μm.

Figure 10*c* shows an SEM image of the typical resulting pore structure. Note that pore sizes vary significantly, but are typically 1 μm or smaller, indicating a roughly 1MHz theoretical frequency response limit as described by Diez-Garias (2002). Also, a 10 kHz loss-less frequency response was demonstrated experimentally with essentially the same porous polymer matrix in Fig. 10*c* is thus more than sufficient for the 1kHz frequency response requirements in Fig. 1 for sublayer control on large hydronautical vehicles.

5.3 *MEKA-5 Top Layer*

The top layer of the MEKA-5 array was fabricated using photolithographic etching and other MEMS mass fabrication processes. This layer provides the 25,600 individual microactuator electrodes and leadouts, grouped into a unit-cell architecture as shown in Fig. 11. The layer was fabricated by a three-mask MEMS process consisting of an "electrodes mask", a "cavities mask", and a "nozzles mask", shown respectively in Figs. 11, and 12*a,b*.

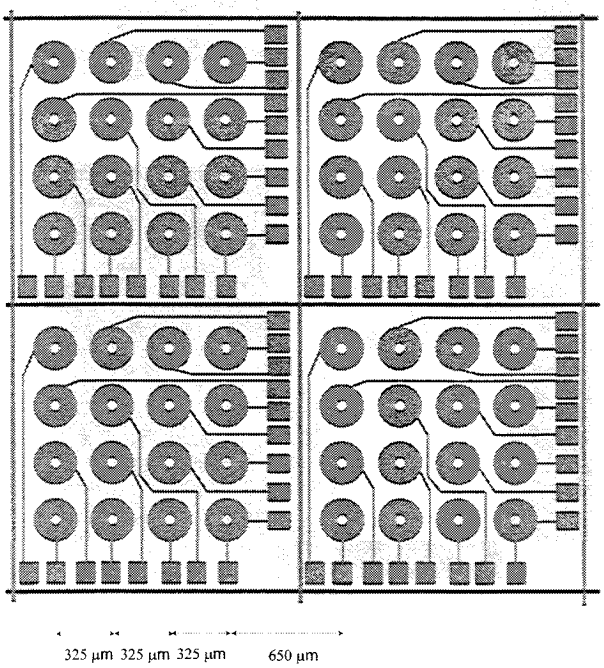

Fig. 11. Layout of top-surface electrodes sublayer mask for 25,600-element MEKA-5 array, showing disk electrodes with leadouts to contacts near edge of each unit cell, and common voltage bus lines running horizontally and vertically between adjacent unit cells.

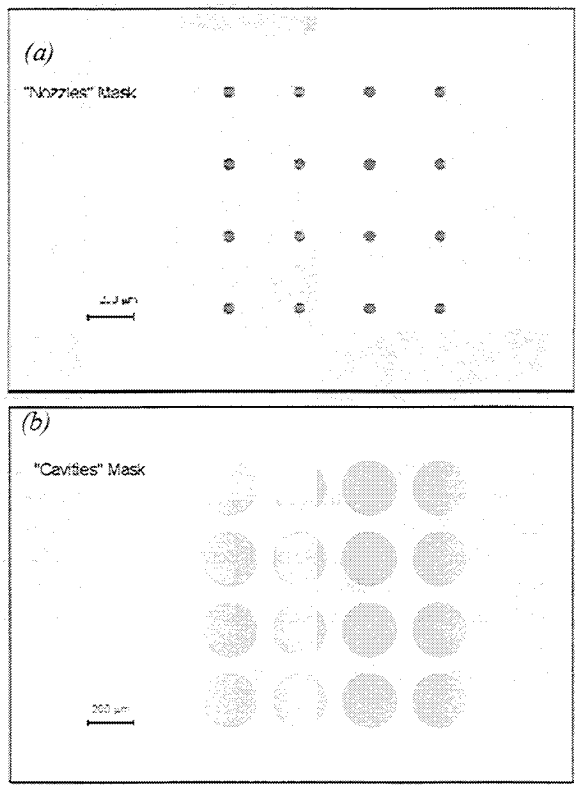

Fig. 12. Additional masks used in MEMS-fabrication of top layer for MEKA-5 hydronautical-scale array, showing *(a)* nozzles mask, and *(b)* cavities mask.

The three component sublayers that make up the top layer are named after the masks used to fabricate them. A full-tile view of the "electrodes sublayer" is shown in Fig. 13*a*. This sublayer provides Cr/Au electrodes for each of the 25,600 individual microactuators and the corresponding leadout for each actuator to a contact located near the edge of its unit cell. A region of this electrodes sublayer is shown in Figs. 13*b*, where the repeated pattern in twenty adjacent units cells can be seen. A closer view of a single unit-cell in this structure is shown in Fig. 13*c*, with the sixteen unit-cell contacts for each of the individual electrodes in the unit cell, together with the common voltage bus lines that run between adjacent unit cells. These voltage bus lines can be readily seen in the edges in Fig. 13*c*. Future versions of this MEKA-5 array could contain a digital signal processing (DSP) layer that selectively connects each of these contacts to the bus line with either positive or negative polarity, depending on the actuation state vector

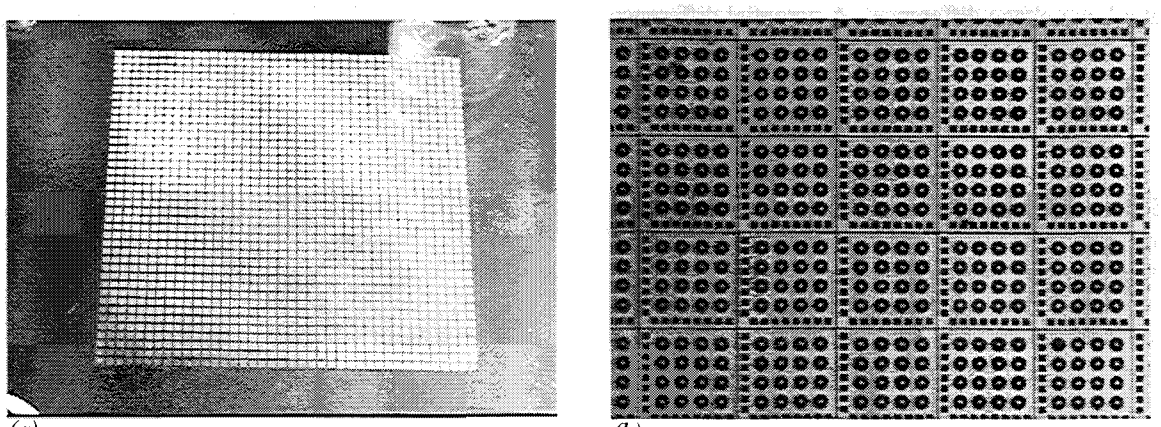

(a) (b)

Fig. 13 (a) Tile-scale view of electrodes sublayer fabricated via the process sequence in Fig. 5.24 for the 25,600-element MEKA-5 hydronautical-scale array. (b) Close-up view of the resulting unit-cell structure in the electrodes sublayer for the 25,600-element MEKA-5 hydronautical-scale array. (c) Unit-cell-scale view of the electrodes sublayer for the 25,600-element MEKA-5 hydronautical-scale array, showing a single unit cell

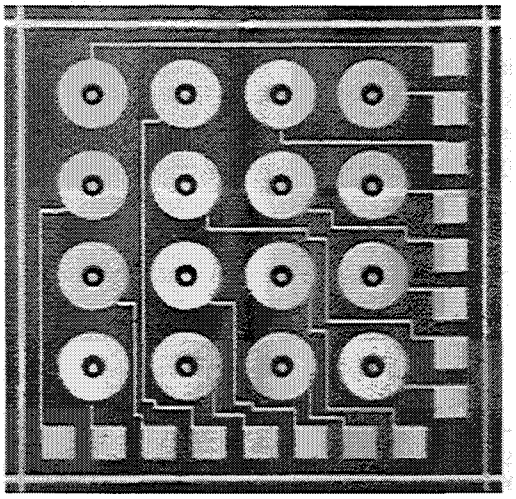

(c)

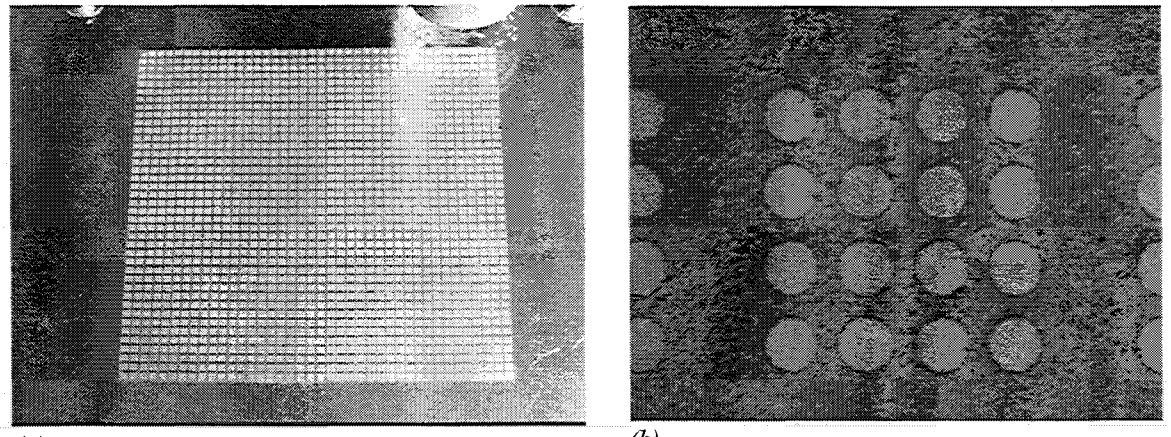

(a) (b)

Fig. 14 (a) Tile-scale view of cavities sublayer fabricated in Su-8 via the process sequence in Fig. 5.24 for the 25,600-element MEKA-5 hydronautical-scale array. (b) Unit-cell-scale view of the cavities sublayer for the 25,600-element MEKA-5 hydronautical-scale array, showing a single unit cell.

implied by the sensor states. As described in §3, this could be readily done via a look-up table approach using a simple programmable logic array (PLA), in place of more traditional control logic approaches based on comparatively elaborate signal processing.

The "nozzles sublayer" is etched in polyamide and provides the 50 μm nozzles through which the pumping induced by the electrokinetic flow occurs. A full view of the "cavities sublayer" is shown in Fig. 14*a*. This sublayer, fabricated in Su-8 material as described in the process flow, serves two specific functions. It provides the necessary structural support for the top layer, and at the same time provides the necessary separation between the top of the porous polymer matrix structure associated each microactuator channel in the center layer and the corresponding top-layer electrode. A closer view of the cavities sublayer in Figs. 14*b* shows the 250 μm diameter cavities on 325 μm center-to-center spacings, and reveals the comparatively well-defined edges of these cavities that result from the fabrication process described above.

5.4 *System Architecture for MEKA-5 Array*

The architecture for arrays like MEKA-5 is based on a 4 × 4 unit-cell composed of wall shear stress sensors and electrokinetic microactuators. The top-surface electrode for each microchannel has a leadout that runs to a contact near the edge of the unit cell. All the unit cells within the tile share a common ground electrode in the bottom layer. A power bus for the entire tile, held at constant reference voltage V_{ref}, runs along horizontal and vertical lines between the active areas of adjacent unit-cells. This redundancy makes the array highly fault tolerant to damage. The look-up table logic circuit provides a three-state bridge between the electrode contact for each of the microactuators and the corresponding closest power bus line. On each clock cycle the actuator state vector $\{A_i\}$ obtained via the programmable logic array from the sensor state vector $\{S_i\}$ sets the voltage $A_i V_{ref}$ of the top electrode for each actuator (see Diez-Garias 2002 for more details). This produces positive volume displacement on some actuators, negative displacements on some actuators, and no action on the remaining actuators. The space between adjacent unit cells on the MEKA-5 array appears sufficient to accommodate the relatively simple circuitry needed to implement this system architecture.

6. Conclusion

Major results and conclusions from the present study of electrokinetic microactuator arrays for active sublayer control in turbulent boundary layers can be summarized as follows:

The present study has been the first to examine the electrokinetic principle as the basis for a new class of microscale actuator arrays for active sublayer control on full scale aeronautical and hydronautical vehicles under realistic operating conditions; the Helmholtz-Smoluchowski scalings that govern such electrokinetic actuator arrays show significant performance advantages from their miniaturization to the microscale.

Specific performance requirements for microactuator spacing, flow rate, and frequency response for active sublayer control have been determined from fundamental scaling laws for the streamwise vortical structures in the sublayer of turbulent boundary layers.

In view of the inherently local nature of the sublayer dynamics, a general system architecture for microactuator arrays appropriate for active sublayer control has been developed based on the concept of relatively small and independent "unit cells", each with their own sensing, processing, and actuation capability, that greatly simplifies the sensing and processing requirements needed to achieve practical sublayer control.

A key innovation in this system architecture is the possibility of replacing previously elaborate control processing requirements with a simple look-up table approach implemented at the unit-cell level, in which a sensor state vector provides the input to a simple programmable logic array (PLA) that determines the corresponding actuator state vector; such an approach is made possible by the comparatively small number of sensors and actuators within each unit cell.

A recently-developed porous polymer fabrication technology has been adapted to permit formation of fine-pore matrix structures suitable for electrokinetic pumping in large, dense arrays of microchannels located in the center layer; porous polymer matrix structures with 1 μm average pore sizes can be readily created within the electrokinetic pumping channels.

Measured volume flow rates produced by such porous polymer-filled electrokinetic microchannels under the effect of steady applied electric fields have been shown to meet the requirements for active sublayer control on full-scale vehicles; the thin layers into which these electrokinetic microactuators can be fabricated permits the required field strengths to be achieved with potential differences of the order of 15-20 V.

Several generations of such electrokinetic microactuator arrays have been built leading to the MEKA-5 full-scale hydronautical array, composed of 25,600 individual electrokinetic microactuators with 350 μm center-to-center spacings, arranged in a 40×40 pattern of unit cells, each composed of a 4×4 matrix of actuators; this array was successfully fabricated in a 7×7 cm^2 tile in 250 μm thick mylar substrate material.

MEMS design and fabrication processes were used to produce a top layer for the MEKA-5 hydronautical-scale array, composed of an electrode sublayer patterned in Cr/Au, a nozzles sublayer etched in polyimide, and a cavities sublayer fabricated in Su-8; the functionality incorporated in this top layer fabrication demonstrates the complete elements needed for microscale electrokinetic actuator arrays for sublayer control.

Acknowledgements

This work was supported by the Defense Advanced Research Projects Agency (DARPA) Microsystems Technology Office under Contract No. F30602-98-2-0228 at The University of Michigan.

References

Burgreen, D. & Nakache, F.R. (1964) Electrokinetic flow in ultrafine capillary slits. *J. Phys. Chem.* **68**, 1084-1091.

Bushnell, D. & McGinley, C. (1989) Turbulent control in wall flows. *Annu. Rev. Fluid Mec*h. **21**, 1-20.

Choi, H., Moin, P. & Kim, J. (1993) Direct numerical simulation of turbulent flow over riblets. *J. Fluid Mech.* **255**, 503-539.

Choi, H., Moin, P. & Kim, J. (1994) Active turbulence control for drag reduction in wall-bounded flows. *J. Fluid Mech.* **262**, 75-110.

Dahm, W.J.A. & Diez-Garias, F.J. (2001) Electrokinetic microactuator arrays for sublayer control in turbulent boundary layers. *Proc. 2nd Int'l. Symp. on Smart Control of Turbulence*, 107-116, University of Tokyo, Tokyo.

Dahm, W.J.A., Paul, P.H., Rakestraw, D.J. & Scherer, J.J. (1997) Fluid microactuators based on the electrokinetic principle. *Bull. Am. Phys. Soc.* **42**, 2247.

Diez-Garias, F.J. (2002) Electrokinetic microactuator arrays for active sublayer control of turbulent boundary layers. *Ph.D. Thesis*, University of Michigan, Ann Arbor, MI.

Diez-Garias, F.J., Dahm, W.J.A. & Paul, P.H. (2000) Microactuator arrays for sublayer control in turbulent boundary layers using the electrokinetic principle. *AIAA Paper 2000-0548*, AIAA, Washington, D.C.

Fiedler, H.E. & Fernholz, H.H. (1990) On management and control of turbulent shear flows. *Prog. Aerospace Sci.* **27**, 305-387.

Gad-el-Hak, M. (1989) Flow control. *Appl. Mech. Rev.* **42**, 261-293.

Gad-el-Hak, M. (1994) Interactive control of turbulent boundary layers: A futuristic overview. *AIAA J.* **32**, 1753-1765.

Gad-el-Hak, M. (1996) Modern developments in flow control. *Appl. Mech. Rev.* **49**, 365-379.

Gad-el-Hak, M. (2001) Flow control: the future. *J. Aircraft* **38**, 402-418.

Ho, C.-M. & Tai, Y.-C. (1996) Review: MEMS and its application to flow control. *J. Fluids Engng.* **118**, 437-447.

Ho, C.-M. & Tai, Y.-C. (1998) Micro-electro-mechanical-systems (MEMS) and fluid flows. *Annu. Rev. Fluid Mech.* **30**, 579-612.

Jacobson, S.A. & Reynolds, W.C. (1993) Active boundary layer control using flush mounted surface actuators. *Bull. Am. Phys. Soc.* **38**, 2197.

Jacobson, S.A. & Reynolds, W.C. (1998) Active control of streamwise vortices and streaks in boundary layers. *J. Fluid Mech.* **360**, 179-211.

Löfdahl, L. & Gad-el-Hak, M. (1999) MEMS applications in turbulence and flow control. *Prog. Aerospace Sci.* **35**, 101- 203.

Lumley, J.L. (1996) Control of turbulence. AIAA Paper 96-0001.

Lumley, J.L. & Blossey, P. (1998) Control of turbulence. *Annu. Rev. Fluid Mech.* **30**, 311-327.

McMichael, J.M. (1996) Progress and prospects for

active flow control using microfabricated electromechanical systems (MEMS). *AIAA Paper 96-0306*, AIAA, Washington, D.C.

Moin, P. & Bewley, T. (1994) Feedback control of turbulence. *Appl. Mech. Rev.* **47**, S3-S13.

Pollard, A. (1997) Passive and active control of near-wall turbulence. *Prog. Aerospace Sci.* **33**, 689-708.

Potter, E.C. (1961) Electrochemistry, Principles and Applications, Cleaver-Hume, London.

Reuss, F. F. (1809) *Memoires de la Societé Imperiale de Naturalistes de Moscou* **2**, 327.

Rice, C.L. & Whitehead, R. (1965) Electrokinetic flow in a narrow cylindrical capillary. *J. Phys. Chem.* **69**, 4017-4023.

Wilkinson, S.P. (1990) Interactive wall turbulence control. In Viscous Drag Reduction in Boundary Layers (Bushnell, D.M. & Hefner, J.N., Eds.) *Prog. Astronautics & Aeronautics* **123**, 479-509, AIAA, Washington, D.C.